

ARTICLE

Received 15 Nov 2014 | Accepted 10 Sep 2015 | Published 23 Oct 2015

DOI: 10.1038/ncomms9601

OPEN

Structurally driven one-dimensional electron confinement in sub-5-nm graphene nanowrinkles

Hyunseob Lim^{1,2,3}, Jaehoon Jung^{1,4}, Rodney S. Ruoff^{2,3} & Yousoo Kim¹

Graphene-based carbon materials such as fullerenes, carbon nanotubes, and graphenes have distinct and unique electronic properties that depend on their dimensionality and geometric structures. Graphene wrinkles with pseudo one-dimensional structures have been observed in a graphene sheet. However, their one-dimensional electronic properties have never been observed because of their large widths. Here we report the unique electronic structure of graphene nanowrinkles in a graphene sheet grown on Ni(111), the width of which was small enough to cause one-dimensional electron confinement. Use of spatially resolved, scanning tunnelling spectroscopy revealed bandgap opening and a one-dimensional van Hove singularity in the graphene nanowrinkles, as well as the chemical potential distribution across the graphene nanowrinkles. This observation allows us to realize a metallic-semiconducting-metallic junction in a single graphene sheet. Our demonstration of one-dimensional electron confinement in graphene provides the novel possibility of controlling its electronic properties not by chemical modification but by ‘mechanical structuring’.

¹Surface and Interface Science Laboratory, RIKEN, 2-1 Hirosawa, Wako, Saitama 351-0198, Japan. ²Center for Multidimensional Carbon Materials, Institute of Basic Science, UNIST-gil 50, Ulsan 689-798, Korea. ³Department of Chemistry, Ulsan National Institute of Science and Technology (UNIST), UNIST-gil 50, Ulsan 689-798, Korea. ⁴Department of Chemistry, University of Ulsan, 93 Daehak-ro, Nam-gu, Ulsan 680-749, Korea. Correspondence and requests for materials should be addressed to Y.K. (email: ykim@riken.jp).

Graphene wrinkles, which are one-dimensional (1D) folded graphene structures, have generally been observed in graphene produced by chemical vapour deposition. These structures have been thought to be the result of the difference in the thermal expansion coefficient between graphene and its substrate¹. A graphene wrinkle is chemically bonded with surrounding planar epitaxial graphene. Therefore, its unique geometric structure is distinct from those of carbon nanotubes² and graphene nanoribbons^{3–6}, which are indisputably 1D structures. Hence, we define a graphene wrinkle as a ‘pseudo 1D structure’ to indicate that it has a 1D shape, but is still a part of a two-dimensional structure.

In the following, we demonstrate the 1D electron confinement in graphene nanowrinkle (GNW) by scanning tunnelling microscopy/spectroscopy (STM/STS), whose width is <5 nm. Moreover, spatially resolved electronic structures have been investigated, and the manipulation of graphene geometry by STM tip has been demonstrated. Our results imply that a semiconducting property can be realized by the mechanical deformation of the graphene geometry not by chemical modification, which is analogous to the case of a strain-induced pseudo magnetic field^{7,8} that was discovered in deformed ‘graphene nanobubbles’⁷. The lack of surface functionalization in our approach can prevent the mobility decline due to chemical defects. Moreover, the covalent bonding at the metallic pEG-semiconducting GNW junction can reduce the contact resistance. Our results demonstrate that the interfacial interaction between graphene and the metal substrate provides a novel way to realize a metallic-semiconducting-metallic junction within a single graphene sheet.

Results

Structural characterization of GNWs. Epitaxial graphene with GNWs was synthesized by dissociating acetylene on a clean Ni(111) surface. A rapid cooling process is necessary, which is the most critical step to synthesize GNWs. Most of the GNWs were observed in the region where the terrace width of the underlying Ni surface was as small as several tens of nanometres (Fig. 1a–c). These GNWs have been recoloured with orange in Fig. 1b, and a line profile along the white arrow in Fig. 1b is plotted in Fig. 1d, which shows that the GNWs on the terrace have larger widths and lower heights than the GNWs at the step edges. We should note that all GNWs were formed at the step edges (red triangles in Fig. 1d) or propagated from kinks at the step edges (blue triangles in Fig. 1d) of the Ni surface, the implication being that the geometrical structure of the underlying Ni must play a crucial role in the formation of GNWs (Supplementary Figs 1–4; Supplementary Note 1,2).

To analyse the structure of the GNWs in detail, we obtained atomically resolved STM images from an isolated GNW on the terrace under different scanning conditions. The top and bottom regions of the GNW in Fig. 1e were scanned at a sample bias (V_s) of 1 V and a feedback current (I_f) of 1 nA, whereas the centre region was scanned with a smaller tip–sample distance ($V_s = 0.05$ V and $I_f = 1$ nA), so that individual carbon atoms could be clearly imaged. Figure 1f was obtained at a much shorter tip–sample distance by increasing I_f up to 6 nA on the same area as Fig. 1e; this clearly shows the graphene lattice of pEG. Both the GNW and pEG areas have the same lattice directions, the indication being that there are no grain boundaries between them. To specify the atomic structure, the height (h) and width (w) of the GNW were precisely measured. The translation vector (**T**), chiral vector (**C_h**) and chiral angle (θ : angle between **T** and the armchair direction) were defined as shown in Fig. 1g. By using the measured values of $w = 2.14$ nm, $h = 0.42$ nm and $\theta \approx 10^\circ$, we could estimate the indices of the **C_h** to be (9, 2) for the GNW (Fig. 1e).

1D electron confinement in GNW. The electronic structures of GNWs located on the terraces of the underlying Ni(111) were investigated by STS and dI/dV mapping. The dI/dV spectrum measured on the GNW (red line in Fig. 2a) by STS measurement included four strong peaks, v_1 and v_2 for the valence band side, and c_1 and c_2 for the conduction band side, the indication being that there were discrete electronic states in the local density of states (LDOS); this behaviour is similar to the ‘band-gap opening’ feature observed in a single-wall carbon nanotube (SWCNT)^{9–11}. There was no evidence of such discrete electronic states on the pEG area (blue line in Fig. 2a). The Dirac point was not clearly apparent, even on the pEG area, because chemisorption on a Ni substrate strongly perturbs the electronic structure of graphene^{12–15}. The dI/dV images in Fig. 2b revealed the spatial distribution of the LDOS, which were obtained at various V_s , including the voltages at peak positions ($V_s = -0.6$ V (v_1) and 0.5 V (c_1)) and between v_1 and c_1 ($V_s = -0.2, 0.01$ and 0.2 V) as well as at the peak positions, the measured dI/dV intensities, which are indicative of the LDOS, were higher on the GNW area than on the pEG area. In contrast, lower LDOSs were observed on the GNW at V_s values in the energy gap between v_1 and c_1 (ΔE_g) (Supplementary Fig. 5 for dI/dV images at the second set of peaks ($V_s = -1.6$ V (v_2) and 1.5 V (c_2)), and V_s between the first and second peaks ($V_s = -1.0$ V and 1.0 V)). The dI/dV images clearly show the metallic-semiconducting-metallic junction across a GNW, which has never been observed in the dI/dV spectra previously measured on other graphene wrinkles^{6,16}.

We considered two plausible origins of these peaks, a strain-induced magnetic field and a 1D electron confinement. An induced magnetic field due to the high curvature in graphene can result in Landau levels in the graphene, as observed in graphene nanobubbles⁷. 1D electron confinement can also result in discrete states (van Hove singularities (vHS)) in electronic structures, a phenomenon that has been extensively investigated in SWCNTs with various chiralities^{2,9–11,17}. To check the first possibility, that is, pseudo-magnetic-field based mechanism, the dI/dV spectra in the present work were compared with Landau levels observed in monolayer graphene under magnetic fields^{18,19}, as well as ones observed in graphene nanobubbles⁷. In a monolayer graphene sheet, zeroth Landau level ($n = 0$) should be observed near Fermi level (E_F), since electrons behave like a Dirac fermion. In addition, the position of the n th Landau level (E_n) follows the relationship $E_n \propto \text{sgn}(n)\sqrt{|n|}$ (ref. 7). In our work, however, discrete energy levels (v_1 or c_1) are too far from the E_F to assign one of them as the zeroth Landau level, even when considering the doping effect. Also, the energy gaps between the peaks do not match the relationship, $E_n \propto \text{sgn}(n)\sqrt{|n|}$. Therefore, we have excluded the pseudo-magnetic-field based mechanism for our results.

To examine the plausibility of the second possible mechanism, that is, 1D electron confinement, we investigated the width dependence on ΔE_g , which should show a relationship to w ($\Delta E_g \propto 1/w$), if ΔE_g originates from 1D electron confinement. Figure 3a shows the dI/dV spectra obtained from the other GNWs within the width range 1.67 nm (a) to 3.65 nm (f; Supplementary Fig. 6). It is apparent that ΔE_g values decreased with increasing widths of the GNWs, but vHS peaks were not observed in GNWs with widths >3.5 nm; note that we tested 26 GNWs, the distribution of which is provided in Supplementary Fig. 7. The width dependence implies that 1D electron confinement is the most plausible explanation for the unique electronic structures of GNWs. To strengthen the 1D electron confinement mechanism, we compared our results with the electronic structures of a SWCNT and a graphene nanoribbon, archetypal 1D carbon materials showing 1D electron confinement phenomena. For a reliable comparison, the actual length for electron confinement (L) is used rather than width of the GNW

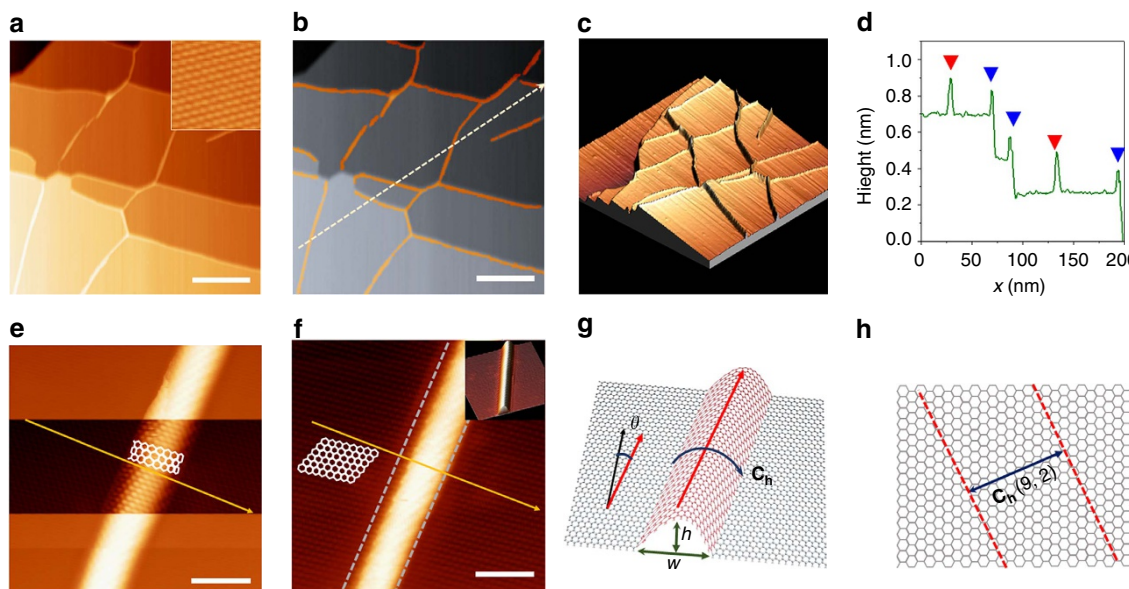


Figure 1 | Atomic structure of GNW. (a–c) STM images of epitaxial graphene on Ni(111). (a) Original image, (inset) graphene lattice on pEG region. Scale bar, 40 nm. (b) Recoloured image showing GNWs with orange colour. (c) Three-dimensional STM image of the epitaxial graphene and GNWs. Scale bar, 40 nm. (d) Height profile along the white dashed arrow in (b). Red triangles and blue triangles indicate the GNWs on the terrace of the Ni(111) surface and at step edges of the Ni(111) substrate, respectively. (e,f) High-resolution STM images with different scanning conditions. (e: top and bottom) $V_s = 1$ V and $I_f = 1$ nA, (centre) $V_s = 0.05$ V and $I_f = 1$ nA. Orange arrows indicate the C_h direction identified in (g) and white hexagonal patterns indicate the carbon atoms. (f) $V_s = 0.05$ V and $I_f = 6$ nA. Scale bars, 2 nm. (g,h) Schematic drawings (g) to clarify the meaning of the parameters used to specify the structure of the GNWs and (h) for the (9, 2) GNW observed in (e,f).

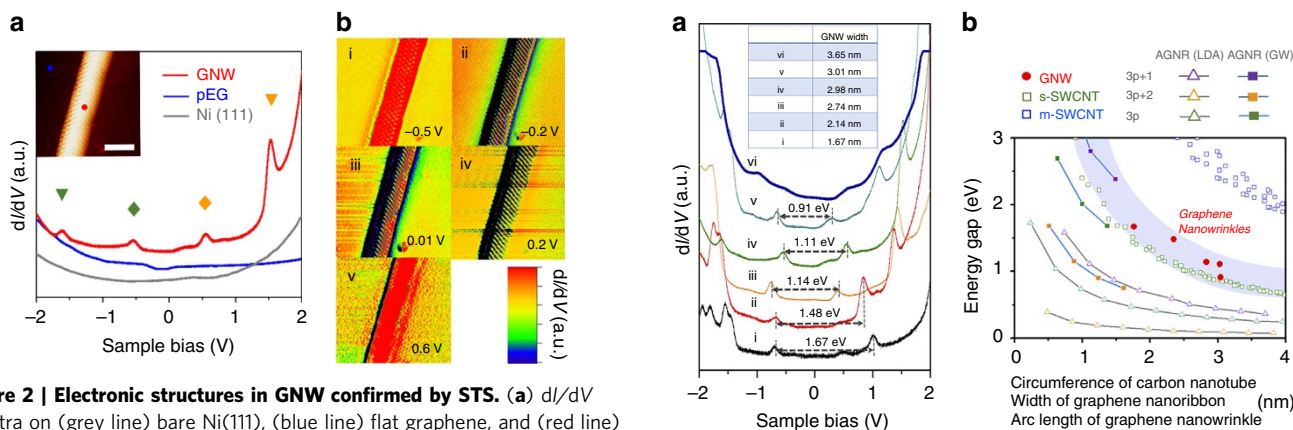


Figure 2 | Electronic structures in GNW confirmed by STS. (a) dI/dV spectra on (grey line) bare Ni(111), (blue line) flat graphene, and (red line) GNW as marked in inset STM image. Scale bar, 2 nm. The symbols above the peaks indicate (green diamond) v_2 , (green triangle) v_1 , (orange triangle) c_1 (from conduction band) and (orange diamond) c_2 . (b) dI/dV mapping images of GNWs obtained at $V_s =$ (i) -0.5 V, (ii) -0.2 V, (iii) 0.01 V, (iv) 0.2 V and (v) 0.6 V.

or the diameter of the SWCNT, because L is more directly related to ΔE_g induced by 1D electron confinement. Hence, ΔE_g s measured in GNWs, and calculated ΔE_g s for both SWCNTs¹⁷ and an armchair graphene nanoribbon (AGNR)^{20,21} are plotted in Fig. 3b as a function of L , that is, arc length of GNW, circumference of SWCNT and width of AGNR, respectively. The arc length of the GNW was estimated on the assumption that the GNW arc shape of its cross section is a part of a circle (Supplementary Figs 8–10; Supplementary Table 1; Supplementary Note 3). The values for SWCNTs are extracted from the Kataura Plot¹⁷, which are calculated by the tight-binding method, and the band gaps of AGNR are estimated by two methods, the local density approximation (LDA)²⁰ and the GW approximation²¹, that are used for comparison. Incidentally, LDA

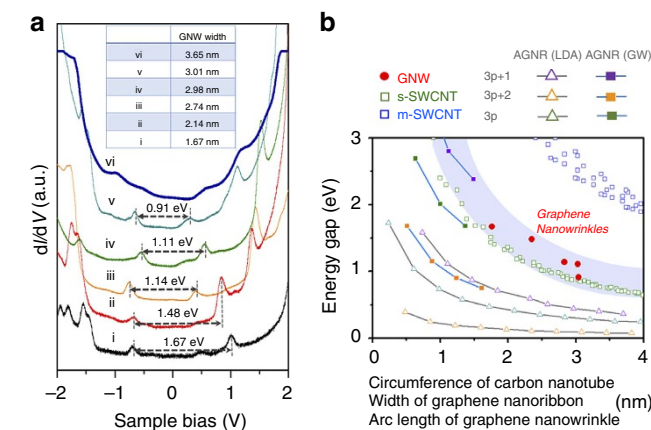


Figure 3 | Width-dependent STS studies in GNWs. (a; i–vi) dI/dV spectra obtained from various GNWs with different widths. (b) Arc-length dependence of energy gap in GNWs, and comparison with calculated values of the peak differences in the SWCNTs and energy gaps in the AGNR. The calculated values for the SWCNTs, AGNR(LDA) and AGNR(GW) were adapted from Kataura *et al.*¹⁷, Son *et al.*²⁰ and Yang *et al.*²¹, respectively.

usually gives underestimated energy values, while GW values for AGNR are expected to be much closer to reality²¹. Figure 3b shows that the ΔE_g s of the GNWs are comparable to the variation of ΔE_g s in AGNR and semiconducting SWCNT, which supports the idea that 1D electron confinement in GNWs is more convincing than a pseudo-magnetic-field based mechanism. However, it is noteworthy that circular boundary conditions in the SWCNT impose an even number of nodes on the wave function along the circumference vector, while the number of nodes can be either even or odd in both GNW and GNR. We therefore believe that the comparison of GNW with GNR is appropriate enough to rationalize our work.

However, further studies would be required not only to fully understand the correlation between ΔE_g and arc length, but also to reveal the other effects on ΔE_g , such as curvature and chirality of the GNW.

Origin of 1D electron confinement in pseudo 1D structure. Although the width dependence verifies the 1D electron confinement in GNWs, it is simply not understood how GNWs

connected with pEG (pseudo one dimensionality) can have the 1D electronic structure. The strong interaction between pEG and the Ni(111) substrate may play a critical role in making a 1D electron channel along GNWs. Owing to the strong interaction, the π orbital of the pEG is hybridized with the d orbital of the Ni surface (π - d hybridization)^{13–15,22}, while pure π orbitals remain at the GNW owing to the freestanding feature of GNW from the Ni surface (Supplementary Fig. 11a). These different degrees of interaction at the interface between pEG and GNW isolate the electronic structure of GNW, which provides the 1D ballistic electron channel along the GNW. It has already been suggested that the spatially different degree of interaction with the substrate is sufficient for inducing local electron confinement in a graphene^{23,24}. Angle-resolved photoemission spectroscopy study has demonstrated the opened bandgap in the graphene sheet on the sidewall facet of a SiC substrate²³. The origin of the local bandgap was explained with the nanoscale electron confinement, which is due to the fact that the nanoscale graphene has non-interacting parts on the sidewall between the graphene-pinned SiC (0001) surface²⁴.

Tao *et al.*⁶ observed a folded graphene structure at the edges of graphene nanoribbons deposited on Au(111), the dimension of which is similar to those of GNWs observed in this study. Nevertheless, vHS peaks induced by 1D electron confinement did not appear, while edge-state peaks appeared near E_F in the dI/dV spectra. This implies that the strong interaction at the pEG is essential for the 1D electron confinement. Because the graphene nanoribbons were physically deposited by a spin-coating method

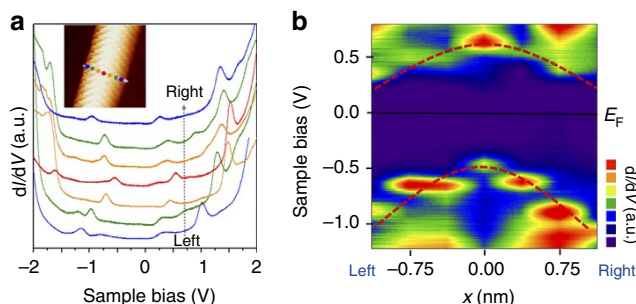


Figure 4 | Spatially resolved-STs studies across GNW. (a) dI/dV spectra measured along the line perpendicular to the GNW direction. Coloured dots in the inset of STM images indicate the positions where the dI/dV spectra were obtained by STS measurement. (b) Spatially resolved-STs map from a with V_s ranging from -1.3 to 0.7 V. Red dotted lines show the behaviour of changes in v_1 and c_1 with respect to their spatial positions.

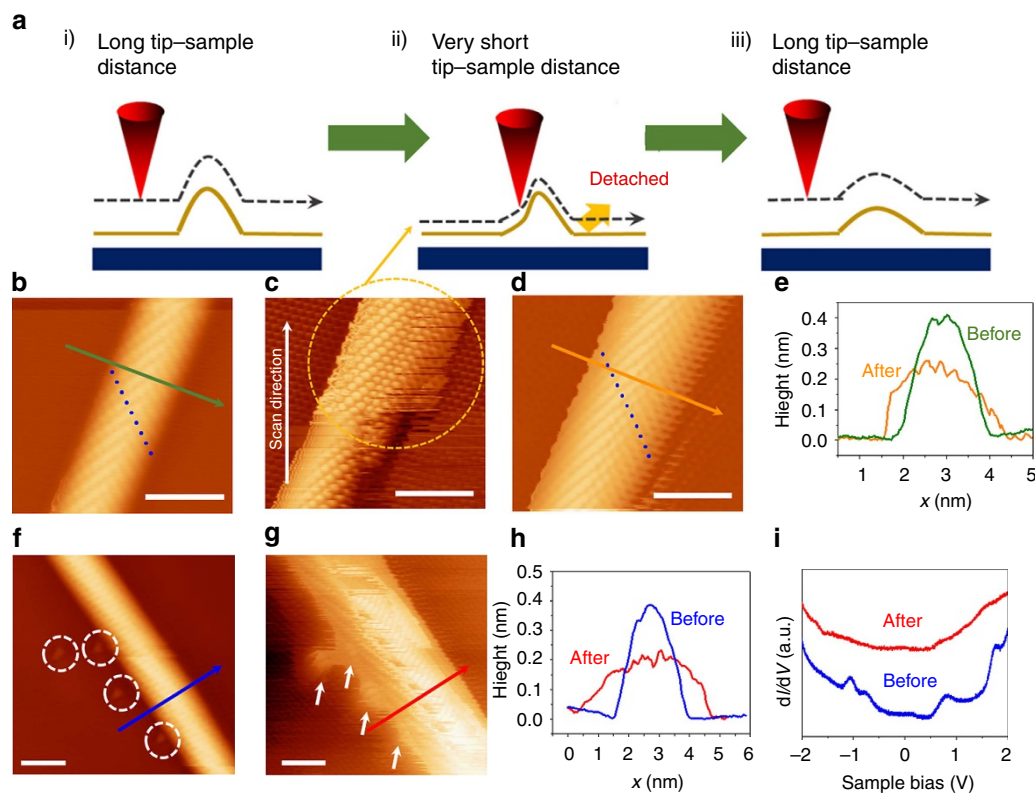


Figure 5 | Manipulation of GNW structure by STM. (a) Schematic illustration of tip-induced manipulation of GNW. (b–d) STM images of GNWs with different scanning conditions for the manipulation. (b) Before the manipulation obtained with $V_s = 0.01$ V and $I_t = 6$ nA. Scale bar, 2 nm. (c) The manipulation process with $V_s = 0.05$ V and $I_t = 6$ nA. Scale bar, 2 nm. (d) After the manipulation obtained with $V_s = 0.01$ V and $I_t = 6$ nA. Scale bar, 2 nm. Blue dots in b and d indicate the positions of carbon atoms along zigzag direction. They reveal the increased number of carbon atoms along zigzag direction of GNW. (e) Height profiles before (b) and after (d) the manipulation. (f–i) Another example of the manipulation showing a substrate defect effect. (f, g) STM images before and after reaction. Scale bars, 2 nm. White-dotted circles in f indicate the substrate defects, and white arrows in g indicate the same positions after the manipulation. (h) Height profiles for (f, g). (i) dI/dV spectra before (f) and after (g) manipulation.

on a Au(111) substrate⁶, the interaction between the graphene nanoribbons and the substrate would have been relatively weak compared with the interaction between the pEGs and Ni(111) in our studies, which might be insufficient for isolating an electronic structure at the folded graphene region.

Spatially resolved-STs studies across GNW. We also investigated changes of electronic structure in a direction perpendicular to the GNW. Spectra of dI/dV were measured at different positions across the GNW (Fig. 4a). It is noteworthy that we could not measure the dI/dV spectrum at the boundary position, because the tunnelling current became unstable when the STM tip was close to the boundary. These spectra were converted to a spatially resolved-STs map (Fig. 4b) within the V_s range -1.3 to 0.7 V. The spatially resolved-STs map revealed that the positions of v_1 and c_1 were shifted along the C_h direction, the indication being that the chemical potential was different. Compared with the centre position of the GNW, the E_{FS} to both the left and right of the centre position were closer to c_1 , the implication being that the chemical potential was larger in the GNW than in the pEG area. We suggest that the asymmetry of the spatially resolved-STs on the left and right sides may be attributed to the asymmetric geometry of the tip. Based on first principles, electron transfer from Ni to epitaxial graphene has been predicted at the epitaxial graphene–Ni contact region^{13,22}. The pEG region interacts strongly with the Ni substrate, the result being electron transfer from the substrate, whereas the GNW is less charged due to the negligible degree of interaction with its substrate. These different degrees of electron transfer determine the electric field across the GNW and may induce the parabolic distribution of c_1 and v_1 in the spatially resolved-STs (Supplementary Fig. 11b).

Manipulation of the GNW structure by the STM tip. Finally, we attempted to manipulate the GNW by the STM tip (Fig. 5a). An STM image of Fig. 5b was obtained with $V_s = 0.05$ V and $I_f = 6$ nA. When the tip was moved closer to the GNW ($V_s = 0.01$ V and $I_f = 6$ nA), the STM image became very unstable (scratched lines appeared), and the width of the GNW became broader (Fig. 5c). Subsequently, Fig. 5d was obtained with the same scanning conditions used to obtain Fig. 5b, and the larger width and smaller height of the GNW were confirmed from the STM image (Fig. 5e). To explain these phenomena, we suggested a tip-induced manipulation mechanism (Fig. 5a). The mechanical force induced by the short distance between the tip and the GNW caused high strain in the GNW. If the induced strain was high enough to overcome the interaction between the pEG and substrate (Fig. 5a (ii)), the pEG beside the GNW can become detached. The result is a larger width and smaller height of the GNW. Figure 5f–i show another example of the manipulation. Several defects are observed near the GNW before the manipulation as marked with white-dotted circles in Fig. 5f. During the manipulation, the detachment of graphene from the underlying Ni substrate more easily occurred on these defects than the other region due to the weak interaction at these points, which resulted in the local deformation of GNW structure as shown in Fig. 5g. The electronic structures before and after the manipulation have been also investigated by STS measurements (Fig. 5i). The pre-existing vHS disappeared in the dI/dV spectrum after the manipulation, which is possibly because the manipulation caused increase of the GNW width larger than the width-limitation (~ 3.5 nm) corresponding the threshold width showing vHS. Another possibility that cannot be excluded is possible modification of the tip apex during the manipulation that can affect the spectral shape to some extent.

Discussion

Our results constitute the demonstration of electron confinement in GNWs with dimensions < 5 nm and the demonstration of an open bandgap, which implies that GNWs have semiconducting properties. Many efforts have been made to manipulate the electronic properties of graphene by chemical modification^{25,26}. In contrast, our study shows a new possibility of controlling the electronic structure of graphene by engineering its geometric structure. Compared with chemical approaches, our approach does not involve the breaking of chemical bonds in graphene layers, which causes the carrier mobility to decrease. Moreover, the metallic pEG and semiconducting GNW are covalently bonded, and their work function should be similar. We therefore suggest that the interface between pEG and GWN will provide Ohmic-like behaviour in electron transport with very low contact resistance (Supplementary Fig. 12). This concept of controlled mechanical deformation does not result in new chemical species but rather in new forms of graphene-based carbons, which consist of only carbon atoms.

Methods

Sample preparation and characterization by STM. The experiments were performed in an ultrahigh-vacuum, low-temperature STM (Omicron LT-STM) at 4.7 K. The Ni(111) single crystal was cleaned by repetitive Ar^+ sputtering-and-annealing cycles. EGs consisting of GNWs were synthesized in an ultrahigh-vacuum chamber (base pressure: 2×10^{-7} Pa) by dissociating C_2H_2 ($P_{C_2H_2}: 2 \times 10^{-5}$ Pa) on Ni(111) at 650 °C for 5 min. For rapidly cooling, the sample was immediately removed from the heating stage after the reaction. All STM images were obtained in a constant-current mode. We measured the differential conductance (dI/dV) with a lock-in amplifier by applying an a.c. bias of 50 mV (797 Hz) to the tunnelling bias. We focused only on the GNWs on the terrace of the Ni(111) surface. A total of 27 individual GNWs were observed with atomically resolved STM images.

References

- Li, X. *et al.* Large-area synthesis of high-quality and uniform graphene films on copper foils. *Science* **324**, 1312–1314 (2009).
- Saito, R., Dresselhaus, G. & Dresselhaus, M. S. *Physical Properties of Carbon Nanotubes* (Imperial College Press, 1998).
- Han, M. Y., Özyilmaz, B., Zhang, Y. & Kim, P. Energy band-gap engineering of graphene nanoribbons. *Phys. Rev. Lett.* **98**, 206805 (2007).
- Li, X. *et al.* Chemically derived, ultrasmooth graphene nanoribbon semiconductors. *Science* **319**, 1229–1232 (2008).
- Wang, X. *et al.* Room-temperature all-semiconducting sub-10-nm graphene nanoribbon field-effect transistors. *Phys. Rev. Lett.* **100**, 206803 (2008).
- Tao, C. *et al.* Spatially resolving edge states of chiral graphene nanoribbons. *Nat. Phys.* **7**, 616–620 (2011).
- Levy, N. *et al.* Strain-induced pseudo-magnetic fields greater than 300 tesla in graphene nanobubbles. *Science* **329**, 544–547 (2010).
- Guinea, F., Katsnelson, M. I. & Geim, A. K. Energy gaps and a zero-field quantum hall effect in graphene by strain engineering. *Nat. Phys.* **6**, 30–33 (2010).
- Wilder, J. W. G. *et al.* Electronic structure of atomically resolved carbon nanotubes. *Nature* **391**, 59–62 (1998).
- Shin, H.-J., Clair, S., Kim, Y. & Kawai, M. Substrate-induced array of quantum dots in a single-walled carbon nanotube. *Nat. Nanotechnol.* **4**, 567–570 (2009).
- Clair, S., Kim, Y. & Kawai, M. Step-edge faceting and local metallization of a single-wall semiconducting carbon nanotube. *J. Appl. Phys.* **110**, 073710 (2011).
- Batzill, M. The surface science of graphene: metal interfaces, CVD synthesis, nanoribbons, chemical modifications, and defects. *Surf. Sci. Rep.* **67**, 83–115 (2012).
- Khomaykov, P. A. *et al.* First-principles study of the interaction and charge transfer between graphene and metals. *Phys. Rev. B* **79**, 195425 (2009).
- Varykhalov, A. *et al.* Electronic and magnetic properties of quasifreestanding graphene on ni. *Phys. Rev. Lett.* **101**, 157601 (2008).
- Dedkov, Y. S., Fonin, M., Rüdiger, U. & Laubschat, C. Rashba effect in the graphene/Ni(111) system. *Phys. Rev. Lett.* **100**, 107602 (2008).
- Guo, Y. & Guo, W. Electronic and field emission properties of wrinkled graphene. *J. Phys. Chem. C* **117**, 692–696 (2012).
- Kataura, H. *et al.* Optical properties of single-wall carbon nanotubes. *Synth. Met.* **103**, 2555–2558 (1999).
- Novoselov, K. S. *et al.* Two-dimensional gas of massless dirac fermions in graphene. *Nature* **438**, 197–200 (2005).
- Zhang, Y., Tan, Y.-W., Stormer, H. L. & Kim, P. Experimental observation of the quantum hall effect and berry's phase in graphene. *Nature* **438**, 201–204 (2005).

20. Son, Y.-W., Cohen, M. L. & Louie, S. G. Energy gaps in graphene nanoribbons. *Phys. Rev. Lett.* **97**, 216803 (2006).
21. Yang, L. *et al.* Quasiparticle energies and band gaps in graphene nanoribbons. *Phys. Rev. Lett.* **99**, 186801 (2007).
22. Giovannetti, G. *et al.* Doping graphene with metal contacts. *Phys. Rev. Lett.* **101**, 026803 (2008).
23. Hicks, J. *et al.* A wide-bandgap metal-semiconductor-metal nanostructure made entirely from graphene. *Nat. Phys.* **9**, 49–54 (2013).
24. Palacio, I. *et al.* Atomic structure of epitaxial graphene sidewall nanoribbons: flat graphene, miniribbons, and the confinement gap. *Nano Lett.* **15**, 182–189 (2015).
25. Liu, J., Tang, J. & Gooding, J. J. Strategies for chemical modification of graphene and applications of chemically modified graphene. *J. Mater. Chem.* **22**, 12435–12452 (2012).
26. Bekyarova, E. *et al.* Advances in the chemical modification of epitaxial graphene. *J. Phys. D* **45**, 154009 (2012).

Acknowledgements

We thank K.S. Novoselov, S. Okada, N. Park, S.R. Hong and Y.-H. Shin for fruitful discussion. H.L. acknowledges the Foreign Postdoctoral Researcher program of RIKEN for financial support. H.L. and R.S.R. were supported by the Institute for Basic Science (IBS), Korea, under the project code of IBS-R019-D1.

Author contributions

H.L., J.J., R.S.R. and Y.K. designed the project, and wrote the manuscript. H.L. synthesized GNW and measured STM and STS. H.L. and J.J. analysed dI/dV data.

Additional information

Supplementary Information accompanies this paper at <http://www.nature.com/naturecommunications>

Competing financial interests: The authors declare no competing financial interests.

Reprints and permission information is available online at <http://npg.nature.com/reprintsandpermissions/>

How to cite this article: Lim, H. *et al.* Structurally driven one-dimensional electron confinement in sub-5-nm graphene nanowrinkles. *Nat. Commun.* 6:8601 doi: 10.1038/ncomms9601 (2015).



This work is licensed under a Creative Commons Attribution 4.0 International License. The images or other third party material in this article are included in the article's Creative Commons license, unless indicated otherwise in the credit line; if the material is not included under the Creative Commons license, users will need to obtain permission from the license holder to reproduce the material. To view a copy of this license, visit <http://creativecommons.org/licenses/by/4.0/>